

ORIGINAL ARTICLE

Expressive architectures enhance interpretability of dynamics-based neural population models

Andrew R. Sedler^{1, 2} | Christopher Versteeg² |
 Chethan Pandarinath^{1, 2}

¹Center for Machine Learning, Georgia Institute of Technology, Atlanta, GA, USA

²Wallace H. Coulter Department of Biomedical Engineering, Emory University and Georgia Institute of Technology, Atlanta, GA, USA

Correspondence

Chethan Pandarinath, Ph.D., Wallace H. Coulter Department of Biomedical Engineering, Emory University and Georgia Institute of Technology, Atlanta, GA, USA
 Email: chethan@gatech.edu

Funding information

This work was supported by NSF Graduate Research Fellowship DGE-2039655 (ARS), the Emory Neuromodulation and Technology Innovation Center (ENTICe), NSF NCS 1835364, DARPA PA-18-02-04-INI-FP-021, NIH Eunice Kennedy Shriver NICHD K12HD073945, NIH-NINDS/OD DP2NS127291, NIH BRAIN/NIDA RF1 DA055667, the Alfred P. Sloan Foundation, and the Burroughs Wellcome Fund (CP), and the Simons Foundation as part of the Simons-Emory International Consortium on Motor Control (CP, CV)

Artificial neural networks that can recover latent dynamics from recorded neural activity may provide a powerful avenue for identifying and interpreting the dynamical motifs underlying biological computation. Given that neural variance alone does not uniquely determine a latent dynamical system, interpretable architectures should prioritize accurate and low-dimensional latent dynamics. In this work, we evaluated the performance of sequential autoencoders (SAEs) in recovering three latent chaotic attractors from simulated neural datasets. We found that SAEs with widely-used recurrent neural network (RNN)-based dynamics were unable to infer accurate rates at the true latent state dimensionality, and that larger RNNs relied upon dynamical features not present in the data. On the other hand, SAEs with neural ordinary differential equation (NODE)-based dynamics inferred accurate rates at the true latent state dimensionality, while also recovering latent trajectories and fixed point structure. We attribute this finding to the fact that NODEs allow use of multi-layer perceptrons (MLPs) of arbitrary capacity to model the vector field. Decoupling the expressivity of the dynamics model from its latent dimensionality enables NODEs to learn the requisite low-D dynamics where RNN cells fail. The sub-optimal interpretability of widely-used RNN-based dynamics may motivate substitution for alternative architectures, such as NODE, that enable learning of accurate dynamics in low-dimensional latent spaces.

KEY WORDS

recurrent neural networks, neural ODEs, dimensionality reduction, dynamical systems, unsupervised learning

1 | INTRODUCTION

Advances in recording technologies over the past decade have enabled simultaneous monitoring of hundreds to thousands of neurons, providing a qualitatively different picture of population activity than was previously available [1, 2, 3]. These high-dimensional recordings often display *latent dynamical structure*, which includes both co-activation across neurons and coordinated evolution over time. In an emerging framework, termed *computation through dynamics*, latent dynamical structure is hypothesized as a key mechanism for implementing biological computations [4, 5, 6]. According to this framework, a neural population constitutes a dynamical system that performs computations through its temporal evolution. Such dynamics have been implicated in computations underlying movement generation, decision making, and working memory [4, 7, 8].

Based on these findings, a promising avenue toward understanding computation in the brain is to build models that can distill latent dynamical structure from recordings of neural activity. Models that accurately capture latent dynamics could be probed via visualization or fixed-point linearization to identify dynamical motifs that implement units of computation [9, 10]. Toward this goal, a variety of methods have been developed to train latent dynamical models that reproduce recorded neural population activity [11, 12, 13, 14, 15, 16]. To date these methods have been highly successful in de-noising activity, for example producing representations of neural activity that correspond with subjects' behaviors on a moment-by-moment basis and millisecond timescale [17, 18, 19]. Yet the degree to which the trained models enable interpretation of the biological circuit's dynamics remain unclear.

To enable interpretation of biological computation, models must recover *accurate* and *parsimonious* representations of dynamics. Neural population models are often trained to reconstruct observed activity, with the assumption that better reconstruction performance corresponds to higher dynamical accuracy. However, because many different dynamical mechanisms could produce the same activity patterns at their output [20], there is no guarantee that a model with high reconstruction performance will have dynamics that match the system being modeled, opening the door to misinterpretation. Thus, it is critical to test whether different architecture choices lead to more accurate models of underlying dynamics. Additionally, empirical evidence suggests that the latent dynamics of neural populations are typically much lower dimensional than the number of neurons we observe [21]. Thus, models of latent dynamics should ideally match the dimensionality of the system being modeled (i.e., be parsimonious) to promote ease of interpretation.

One recent approach, Poisson Latent Neural Differential Equations (PLNDE [14]), adapted neural ordinary differential equations (NODEs [22]) for the statistics of neural spiking data. PLNDE demonstrated impressive performance in recovering low-dimensional phase portraits and fixed points of nonlinear dynamical systems with few trials and low firing rates. While this work hinted that NODE-based models may perform better than recurrent neural network (RNN)-based models at lower latent state dimensionalities, it remains unclear how the NODE compares directly to the RNN, and what features of NODEs are responsible for the differences. A salient difference between RNNs and NODEs is that the capacity of an RNN is tied to its latent dimensionality, while NODEs can define vector fields using networks of arbitrarily high capacity. This might enable NODE-based models to more easily learn dynamics in low-dimensional spaces, which would explain their performance advantage in that regime.

In this work, we evaluate the performance of RNN-based and NODE-based SAEs in recovering three latent chaotic attractors from simulated spiking datasets. We quantify the accuracy of inferred firing rates using the data log-likelihood and the true rate R^2 . We also introduce a metric, hidden R^2 , which measures the fraction of inferred latent state variance explained by an affine transformation of the true latent states. Despite their success in reconstructing neural activity patterns [17, 18, 13], we find that RNN-based SAEs require many more latent dimensions than the synthetic systems they are attempting to model. Moreover, we find that the dynamics learned by the RNNs

are a poor match to the synthetic systems, in that a large fraction of the models' variance reflects activity not seen in the synthetic system. Finally, we find that the behavior of RNNs linearized around their fixed points is qualitatively different from that of the true systems.

In contrast, we find that NODE-based SAEs learn dynamics in the true latent dimensionality with minimal superfluous dynamics, while capturing the behavior of the true system around its fixed points. These results indicate that the higher capacity available to NODEs, particular in lower dimensions, enables them to learn the requisite dynamics where RNN cells fail. The suboptimal interpretability of widely-used RNN-based dynamics may motivate substitution for alternative architectures, like the NODE, that enable learning of accurate dynamics in low-dimensional latent spaces. Future models could leverage these characteristics to learn simpler, more interpretable latent dynamics that elucidate the computational mechanisms implemented by real neural populations.

2 | RELATED WORK

Converging theoretical and experimental evidence suggests that the time-course of neural activity can be modeled as a dynamical system whose state variables are not individual neurons, but instead a lower-dimensional set of latent variables [16, 23]. In this paper we restrict analyses to systems that are well-modeled as autonomous dynamical systems, which can be described in continuous time as:

$$\frac{dz}{dt} = f(z) \quad x = \text{Poisson}(\exp(g(z)))$$

Where $z \in \mathbb{R}^D$ is the latent state, $x \in \mathbb{R}^N$ is the observed neural population activity, f defines the latent dynamics that determine the time-evolution of the system, and g defines the mapping from latent variables to neural activity. As neurons cannot have negative firing rates, we make outputs from g positive using \exp and follow with Poisson sampling to determine the number of times each neuron spikes in each time bin.

Early efforts to explicitly model the latent dynamics of neural populations imposed strict limitations on dynamical complexity by representing f using a linear dynamical system (LDS) and g using a linear readout for tractability and ease of interpretability [24]. Subsequent approaches allowed more flexibility in g , enabling models to explain more variance in neural data while maintaining linear dynamics [25]. Still other approaches have used switching linear dynamical systems (SLDS) to approximate nonlinear dynamics in f [11, 26].

The field of dynamical system identification has had great success in recovering governing equations from time series measurements, particularly in the physics domain [27, 28, 29]. However, existing approaches rely heavily on sparse, symbolic regression from states to derivatives [27], which poses a number of problems for spiking datasets. First, discrete counts and their derivatives are not suitable for regression and naive smoothing approaches are unlikely to preserve dynamically relevant features. Second, it is unclear whether the dynamics of neural populations can or should be described by a sparse selection from a library of nonlinear terms.

With the resurgence of deep learning over the past decade, a powerful class of methods has emerged that use RNNs to approximate f [17, 18, 30, 13]. In head-to-head comparisons, RNN-based methods replicate neural activity patterns with substantially higher accuracy than LDSs on datasets from a variety of brain areas and behaviors, suggesting that linear dynamics may not adequately model the dynamics of neural systems [23]. A recent model combined the RNN and SLDS architectures to improve the RNN's interpretability, but it is unclear how this model compares to standard RNNs in recovering latent dynamics [31].

Early characterization of the dynamics of RNN-based models for interpretability began with fixed-point linearizations of networks trained to perform simple tasks, such as 3-bit memory and pattern generation [9]. Subsequent work has used similar techniques to elucidate the computational dynamics underlying text classification and to illustrate commonalities among different types of RNNs trained to perform the same task [32, 33].

The goal of this work is to directly compare RNN-based and NODE-based SAEs to clearly present the benefits of more interpretable architectures for neural population models.

3 | METHODS

3.1 | Datasets

To determine whether trained models accurately recapitulate latent dynamical rules from observed population activity, we require reference datasets where the ground truth dynamics are known. Accordingly, we set up synthetic test cases that mimic empirical properties of neural systems, i.e., low-D latent dynamics that are observed via noisy spiking activity of neural populations. We created each synthetic dataset based on a long simulated trajectory of a chaotic dynamical system ($D = 3$; see Supplementary Table 1). To generate firing rates for $N = 10$ neurons, the trajectory was first projected through a $D \times N$ random matrix with elements sampled from $U[-0.5, 0.5]$. The resulting data were standardized to zero-mean and unit variance and passed through an exponential activation function, resulting in N time-varying firing rates. To simulate spiking activity, firing rates were sampled as inhomogenous Poisson processes. From this spiking data, 1600 segments of length $T = 70$ were randomly split into training ($1280 \times T \times N$) and validation ($320 \times T \times N$) datasets.

3.2 | Model Architecture

All models used in this work were variations of a sequential autoencoder (SAE). Briefly, the binned spike counts, $\mathbf{X} \in \mathbb{R}^{T \times N}$, were fed into a 64-unit bidirectional GRU, whose final hidden states were linearly projected to an initial condition, \mathbf{z}_0 .

$$\mathbf{h}_T = \text{BiGRU}(\mathbf{X})$$

$$\mathbf{z}_0 = \mathbf{W}_E \mathbf{h}_T + \mathbf{b}_E$$

The initial condition was unrolled by the dynamics model (f , GRU or NODE) to compute the time-varying latent states, \mathbf{z}_t , which were projected to inferred rates, \mathbf{y}_t , by a linear-exponential readout.

$$\begin{aligned} \mathbf{z}_t &= \text{GRU}(\mathbf{z}_{t-1}) \quad \text{OR} \quad \mathbf{z}_t = \mathbf{z}_{t-1} + \int_{t-1}^t \text{NODE}(\mathbf{z}(t)) dt \\ \mathbf{y}_t &= \exp(\mathbf{W}_R \mathbf{z}_t + \mathbf{b}_R) \end{aligned}$$

We use standard GRU cells throughout the model (see Supplementary Material). The NODE consisted of an MLP with one hidden layer of 128 ReLU units. For the GRU, it is important to note that both model capacity and dimensionality of the latent space are determined by the number of hidden units, and dynamics are determined by

the recurrent connectivity. On the other hand, the NODE separates hidden dimensionality from model capacity and explicitly models dynamics by approximating a vector field using an MLP.

$$\text{NODE}(\mathbf{z}) = \mathbf{W}_2 \text{ReLU}(\mathbf{W}_1 \mathbf{z} + \mathbf{b}_1) + \mathbf{b}_2$$

Networks were trained to maximize the Poisson log-likelihood of the observed data, $\mathbf{X} = [\mathbf{x}_1 \dots \mathbf{x}_T]^T$, given the inferred firing rates, $\mathbf{Y} = [\mathbf{y}_1 \dots \mathbf{y}_T]^T$. While GRU outputs were computed with a fixed time step, NODE trajectories were computed using the Tsit5 solver and were trained incrementally to avoid dynamical collapse to the origin. Rather than compute loss on the whole trajectory, we added five new time steps every 150 epochs, up to the max of 70 steps. All networks were trained via backpropagation through time. Further training details are given in the Supplementary Material.

$$L_\theta(\mathbf{Y}) = -\frac{1}{TN} \sum_{t=1}^T \sum_{n=1}^N \log \text{Poisson}(x_{t,n} | y_{t,n})$$

3.3 | Metrics

All metrics were evaluated on validation data. Reconstruction performance was evaluated by two key metrics. The first, spike negative log-likelihood (NLL), was the same as the Poisson NLL used during model training. The second, rate R^2 , was the coefficient of determination between true and inferred firing rates, averaged across neurons. While these metrics capture similar information, we use both because spike NLL is the only metric available for real datasets, but rate R^2 captures the model's ability to denoise the data.

While reconstruction performance evaluates how well the inferred latent states explain the variance in the neural data, it is blind to variance in the inferred latent states that is not explained by the true latent states. We introduce a new metric, hidden R^2 , that provides a complementary view of the accuracy of the inferred latent states. Hidden R^2 measures the fraction of inferred latent state variance explained by an affine transformation of the true latent states. Taken together, rate R^2 and hidden R^2 indicate whether models are inferring the latent features of the true system, without inventing superfluous features that could hinder interpretability.

4 | RESULTS

4.1 | Neural ODEs learn more accurate and parsimonious representations of dynamics

We trained RNN-based and NODE-based SAEs to model the latent dynamics underlying synthetic datasets, for which ground truth firing rates, latent states, and fixed points were known. We created a synthetic dataset by projecting an Arneodo system trajectory into an observation space and sampling binned spike counts (Fig. 1a; see Methods). The Arneodo system is a mildly chaotic 3-D attractor based on a modified Lotka-Volterra ecosystem (see Supplementary Material). We chose this system because (1) it demonstrates relatively limited chaotic behavior [34] and (2) regions around its fixed points are well-sampled by the latent trajectories, making them more easily identifiable.

We evaluated reconstruction performance as a function of hidden size for GRU-based and NODE-based autoencoders (Fig. 1b). The reconstruction performance of both model types increased with hidden size, but the GRU

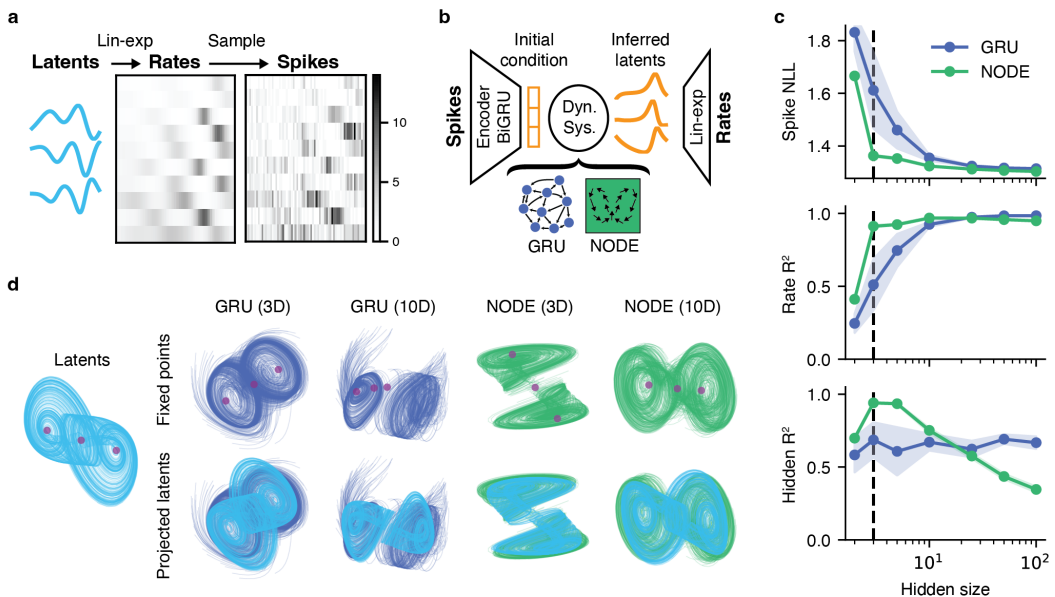


FIGURE 1 Reconstruction of Arneodo system using GRUs and NODEs. (a) The data generation pipeline for a single sample consisted of projecting trajectories through a random linear projection, followed by exponentiation and Poisson sampling. (b) A schematic showing the architecture of GRU-based and NODE-based SAEs used in these experiments. (c) Performance metrics for models of differing sizes. Traces are means and shaded regions are standard deviations across model initializations ($N = 5$). Vertical line indicates the true latent dimensionality. (d) Latent trajectories inferred by each model (or top-3 PCs), overlaid with learned fixed points (top) and with the latent projection used to compute hidden R^2 (bottom).

consistently required higher dimensionality to achieve similar reconstruction performance to the NODE. For example, GRU-based models required a hidden size of 10 in order to match the performance of the 3-D NODE (Fig. 1c, top and middle). This indicates that NODEs are better suited than GRUs for modeling dynamics in low-dimensional latent spaces.

While low-dimensional GRUs do not have sufficient capacity to model the data, it is possible that high-dimensional GRUs could recover the low-dimensional attractor embedded in a higher-dimensional state space. In this case, we would expect the true latent states to explain the variance in the inferred latent states. To quantify this phenomenon we introduce a new metric, hidden R^2 (see Methods), which evaluates the fraction of the variance of inferred latent states explained by an affine transformation of the true latent states. In combination with reconstruction performance, it allows us to determine which models are recovering the true latent trajectories without inventing dynamics that do not exist in the true system.

Despite accurate reconstruction performance at high dimensionalities, GRUs exhibited poor hidden R^2 for all models, remaining relatively flat across hidden sizes and peaking at $R^2 = 0.69$ for the 50-D model. This implies that, even as larger GRUs exhibited high reconstruction performance, a substantial fraction of the GRU's variance remained inconsistent with the true dynamics. In contrast, the 3-D NODE scored highest by our hidden R^2 metric ($R^2 = 0.94$) in comparison to all tested alternatives, and increasing the latent size to 5-D caused only a minor decrease (Fig. 1c, bottom). For these models, the variance in NODE states could be explained almost exclusively by the true latent

states. The 2-D NODE had low hidden R^2 because it was not able to capture the true system, and larger NODEs saw gradual declines as models increasingly relied on inaccurate dynamics.

The superfluous and inaccurate dynamics of the GRU models were evident in visualizations of the inferred latent trajectories (Fig. 1d). The presence of inaccurate dynamics despite high reconstruction performance provides a warning for interpreting the dynamics of these models in real neural datasets, where no ground truth latent system exists and hidden R^2 cannot be evaluated. In such cases, analysis of inaccurate dynamics could lead to erroneous conclusions about the computational mechanisms of the neural population.

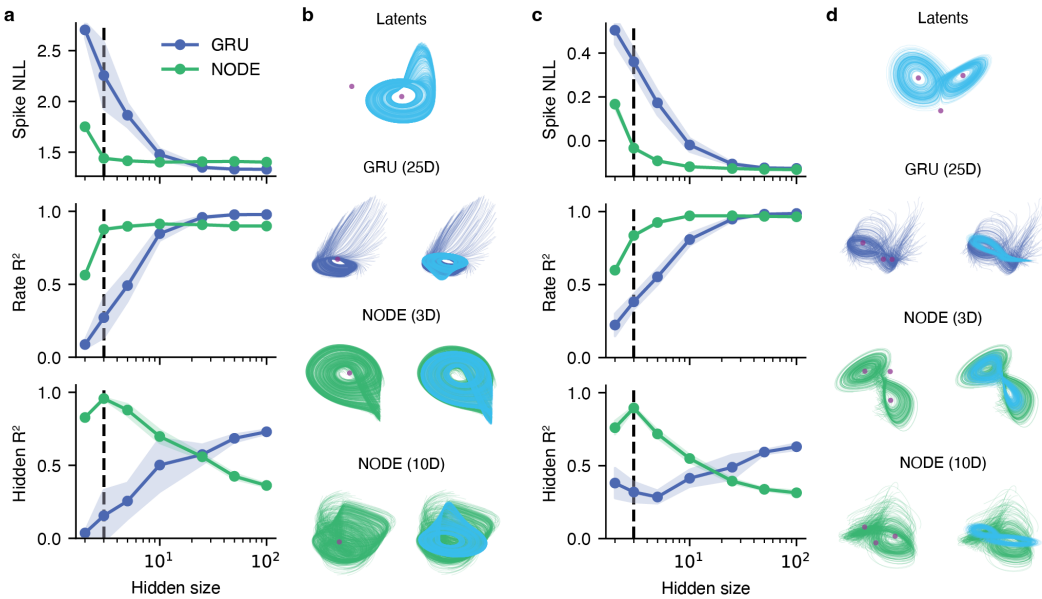


FIGURE 2 Reconstruction of Rössler and Lorenz systems using GRUs and NODEs. (a) Performance metrics for models trained on the Rössler dataset. Traces are means and shaded regions are standard deviations across model initializations ($N = 5$). (b) Latent trajectories inferred by each model for the Rössler dataset (or top-3 PCs), overlaid with learned fixed points (left) and with the latent projection used to compute hidden R^2 (right). (c-d) Same as (a-b), for the Lorenz dataset.

4.2 | Neural ODEs learn better representations of dynamics across systems

We next applied the same SAE models and analysis to synthetic data from two additional dynamical systems, the Rössler and Lorenz attractors (see Supplementary Material), and found that NODE continued to achieve high reconstruction performance with fewer latent dimensions and fewer superfluous dynamical features than the GRU (Fig. 2). Hidden R^2 was clearly the highest for the NODE-based models with the correct dimensionality (3-D) across all datasets. However, in real neuroscientific datasets, the "correct" dimensionality is unknown and hidden R^2 is unavailable, thus model selection would have to rely on spike NLL. For the Rössler and Arneodo systems, the spike NLL of the NODE produced an elbow at the correct dimensionality (Figs. 2a, top and 1c, top), which could serve as a guide for selecting the appropriate dimensionality. However, NODE models of the Lorenz system tended to overestimate

latent dimensionality, as 5-D and 10-D models performed substantially better than 3-D (Fig. 2d, top).

For Rössler and Lorenz systems, GRU hidden R^2 performance tended to increase with dimensionality up to a plateau, which likely reflected an increasing ability to fit the data. The fact that GRU required such high dimensionality to fit simple 3-D systems makes it unlikely to be an interpretable model of real neural systems. Notably, hidden R^2 on the Lorenz dataset plateaued and began to decline for models larger than 100 hidden units (not shown).

4.3 | Neural ODEs more effectively recover fixed point properties

Going beyond comparing trajectories, the fixed points (FPs) of nonlinear dynamical systems are useful interpretability tools because they identify topologically important, locally linear regions where the system Jacobian can be decomposed to identify dynamical modes. The linearized dynamics around an FP indicate whether a nearby trajectory will diverge from ($||\lambda_i|| > 1$), converge to ($||\lambda_i|| < 1$), or oscillate around ($\Im(\lambda_i) > 0$) that FP along a given eigenvector, v_i , providing a qualitative and succinct description of the system's dynamics in that region. By pairing learned FPs to their corresponding true FPs and comparing eigenvalues, we reveal more fine-grained information about whether the learned dynamics have similar behavior to the true system.

For each dataset, we selected representative low-dimensional and high-dimensional models with GRU-based and NODE-based dynamics. All of these models achieved high reconstruction performance, with the exception of the low-dimensional GRUs. For each model, we found a set of FPs by minimizing the norm of the vector field, as demonstrated in previous work [9, 35]. This approach identified three FPs for Arneodo and Lorenz datasets and one FP for the Rössler dataset in all models with high reconstruction performance. At each FP, we computed the discrete-time Jacobian of the corresponding dynamics model. Discrete-time Jacobians for the true systems were computed analytically. All Jacobians were decomposed to their eigenvalues, which were the subjects of analysis. Learned FPs were trivially mapped to the corresponding true FPs based on their eigenspectrum. For Arneodo and Lorenz datasets, we analyzed only one FP from each symmetric pair. We compare the properties of each learned FP to those of the corresponding true FP by overlaying plots of their eigenvalues in the complex plane (Fig. 3).

Models learned FPs analogous to those of the true systems with varying degrees of fidelity. The low-D NODE matched FPs and their qualitative behavior very well overall (Fig. 3d). On the other hand, the low-D GRU was not able to reconstruct the data or adequately recover FPs on any of the datasets (Fig. 3b). For example, the model learned lobe FPs with unstable oscillations ($||\lambda_i|| > 1$) instead of the stable oscillations of the true system ($||\lambda_i|| < 1$). The high-D GRU achieved good reconstruction performance, but in all cases developed FPs with many attracting dimensions ($||\lambda_i|| < 1$) (Fig. 3c). These additional attractive mechanisms allowed the initial conditions to be placed far away from the regions of state space frequented by the model, creating the trailing trajectories visible in the PCA projections (Fig. 1d). A more accurate model would have mostly stable dimensions ($\lambda_i \approx 1$), which would prevent trailing trajectories and force initial conditions to be placed closer to their true locations in state space. The high-D NODE captured the core properties of the fixed points well in most cases, but tended to develop superfluous stable oscillations ($||\lambda_i|| < 1$ and $\Im(\lambda_i) > 0$) (Fig. 3e) which were also visible in the PCA projections (Fig. 1d). All NODE and GRU models struggled to capture the central Lorenz FP, which had few nearby trajectories. Similarly, all models failed to capture a Rössler FP that was distant from the system's trajectories. We believe this to be a limitation of the dataset, where the dynamics near some fixed points are underdetermined for the given trajectories, and highlights the need for more comprehensive sampling of latent state spaces for robust fixed point recovery.

5 | DISCUSSION

Neural population models based on ANNs have shown great success in reproducing neural activity patterns and relating brain activity to behavior. Previous work had speculated that learned dynamics might contain useful information about neural computation, but this idea had not been investigated in detail. In parallel, techniques had been developed for understanding computation in task-trained RNNs via fixed points. In this work, we combined these methods to investigate the challenges surrounding recovery of latent dynamical systems with ANNs. We demonstrated issues with widely-used GRU-based architectures and illustrated how the separation of latent size and expressivity allows NODE-based SAEs to accurately model low-dimensional latent dynamics underlying simulated neural activity. By testing our models on multiple datasets, we also provided insight into how neural dataset properties can affect dynamical recovery. We demonstrated that dynamics which are highly sensitive to initial conditions (i.e., chaotic) are more difficult to recover in their true latent dimension, as larger latent spaces become increasingly useful as trajectories become harder to predict. We also showed that global dynamics may be underdetermined given a limited set of locally sampled latent trajectories, resulting in incomplete recovery of fixed points distant from the sampled area. These findings will inform the design of more interpretable dynamics-based neural population models to provide insight into the dynamics that drive biological computation.

Our finding that models sometimes overestimated latent dimensionality by achieving substantially higher performance with larger latent spaces (e.g., for the Lorenz system, Fig. 2d, top) was surprising. We suspect this issue may relate to the level of chaos in a given system. For the systems tested, the different maximum Lyapunov exponents, which characterize the rate of divergence of infinitesimally close initial conditions, support this idea. For Rössler, Arneodo, and Lorenz, they are 0.076, 0.243, and 1.091 respectively [36, 34, 37, 38]. We hypothesize that extra model dimensions may provide performance gains in the presence of chaos by allowing correction of divergent trajectories caused by small initial condition placement errors.

While these simulations are a reasonable starting point, real neural populations receive input from other areas that can drive the state independently from the internal dynamics of the population. One limitation of this work is that it does not tackle the problem of inferring inputs to the latent dynamical system. This problem is difficult due to essential ambiguities about whether a given change in state is driven by inputs or internal dynamics. While some progress has been made by imposing reasonable priors on inputs for RNN-based models [12, 17], more work is necessary to develop an analogous approach for NODEs. Additionally, we use linear readouts for both data generation and modeling, which may not adequately capture the complexity of real neural manifolds. Using a linear readout on neural data that lies on a nonlinear manifold could impose additional burden on the latent dynamics model, in the form of higher dimensionality or higher complexity. Investigation of alternative readouts may be a promising direction for future work. Finally, while NODE-based SAEs reduce the risk involved in model selection, the models with the best reconstruction performance are not guaranteed to most concisely capture the true dynamics. This problem may be an unavoidable consequence of increasing model capacities.

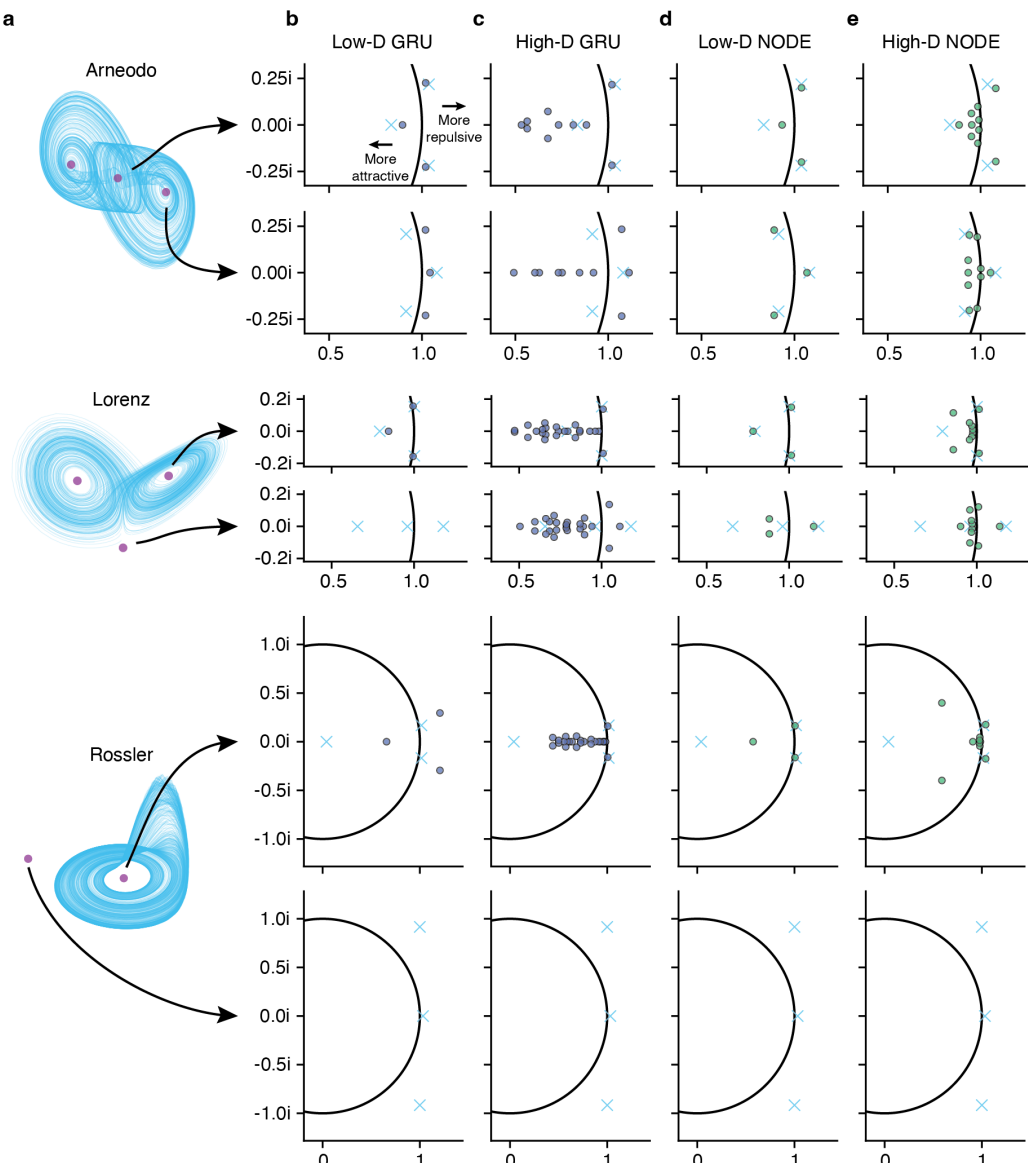


FIGURE 3 Recovery of fixed points and their properties using GRUs and NODEs. (a) True latent trajectories and fixed point locations for the three modeled systems. (b) Fixed points of trained networks were found by gradient descent on the norm of the learned vector field. Discrete-time Jacobians were computed for each fixed point of each network on each dataset. Jacobian eigenvalues are plotted here in the complex plane for the 3-D GRUs. Cyan markers indicate the true system eigenvalues. (c) Same as (b) for the 10-D GRU (Arneodo) and 25-D GRUs (Lorenz and Rossler). (d) Same as (b) for the 3-D NODEs. (e) Same as (b) for the 10-D NODEs.

references

- [1] Stevenson IH, Kording KP. How advances in neural recording affect data analysis. *Nature Neuroscience* 2011 Feb;14(2):139–142.
- [2] Juavinett AL, Bekheet G, Churchland AK. Chronically implanted Neuropixels probes enable high-yield recordings in freely moving mice. *eLife* 2019;8:e47188.
- [3] Jun JJ, Steinmetz NA, Siegle JH, Denman DJ, Bauza M, Barbarits B, et al. Fully integrated silicon probes for high-density recording of neural activity. *Nature* 2017 Nov;551(7679):232–236. <https://www.nature.com/articles/nature24636>, number: 7679 Publisher: Nature Publishing Group.
- [4] Vyas S, Golub MD, Sussillo D, Shenoy KV. Computation Through Neural Population Dynamics. *Annual Review of Neuroscience* 2020;43(1):249–275. <https://doi.org/10.1146/annurev-neuro-092619-094115>, _eprint: <https://doi.org/10.1146/annurev-neuro-092619-094115>.
- [5] Shenoy KV, Kao JC. Measurement, manipulation and modeling of brain-wide neural population dynamics. *Nature Communications* 2021 Jan;12(1):633. <https://www.nature.com/articles/s41467-020-20371-1>, number: 1 Publisher: Nature Publishing Group.
- [6] Khona M, Fiete IR. Attractor and integrator networks in the brain. *Nature Reviews Neuroscience* 2022;p. 1–23.
- [7] Shenoy KV, Sahani M, Churchland MM. Cortical control of arm movements: a dynamical systems perspective. *Annual Review of Neuroscience* 2013 Jul;36:337–359.
- [8] Jazayeri M, Ostojevic S. Interpreting neural computations by examining intrinsic and embedding dimensionality of neural activity. *arXiv*; 2021.
- [9] Sussillo D, Barak O. Opening the black box: low-dimensional dynamics in high-dimensional recurrent neural networks. *Neural Computation* 2013 Mar;25(3):626–649.
- [10] Driscoll L, Shenoy K, Sussillo D. Flexible multitask computation in recurrent networks utilizes shared dynamical motifs. *bioRxiv* 2022;.
- [11] Linderman S, Johnson M, Miller A, Adams R, Blei D, Paninski L. Bayesian Learning and Inference in Recurrent Switching Linear Dynamical Systems. In: Proceedings of the 20th International Conference on Artificial Intelligence and Statistics PMLR; 2017. p. 914–922. <https://proceedings.mlr.press/v54/linderman17a.html>, iSSN: 2640-3498.
- [12] Sussillo D, Jozefowicz R, Abbott LF, Pandarinath C. LFADS - Latent Factor Analysis via Dynamical Systems. *arXiv*; 2016.
- [13] Schimel M, Kao TC, Jensen KT, Hennequin G. iLQR-VAE : control-based learning of input-driven dynamics with applications to neural data. *bioRxiv*; 2021.
- [14] Kim TD, Luo TZ, Pillow JW, Brody C. Inferring latent dynamics underlying neural population activity via neural differential equations. In: International Conference on Machine Learning PMLR; 2021. p. 5551–5561.
- [15] Hurwitz C, Kudryashova N, Onken A, Hennig MH. Building population models for large-scale neural recordings: Opportunities and pitfalls. *Current Opinion in Neurobiology* 2021;70:64–73.
- [16] Duncker L, Sahani M. Dynamics on the manifold: Identifying computational dynamical activity from neural population recordings. *Current Opinion in Neurobiology* 2021 Oct;70:163–170. <https://www.sciencedirect.com/science/article/pii/S0959438821001264>.
- [17] Pandarinath C, O’Shea DJ, Collins J, Jozefowicz R, Stavisky SD, Kao JC, et al. Inferring single-trial neural population dynamics using sequential auto-encoders. *Nature Methods* 2018 Oct;15(10):805–815. <https://www.nature.com/articles/s41592-018-0109-9>, number: 10 Publisher: Nature Publishing Group.

- [18] Keshtkaran MR, Sedler AR, Chowdhury RH, Tandon R, Basrai D, Nguyen SL, et al. A large-scale neural network training framework for generalized estimation of single-trial population dynamics. *Nature Methods* 2022;19(12).
- [19] Zhu F, Grier HA, Tandon R, Cai C, Agarwal A, Giovannucci A, et al. A deep learning framework for inference of single-trial neural population activity from calcium imaging with sub-frame temporal resolution. *Nature Neuroscience* 2022;19(12).
- [20] Kao JC. Considerations in using recurrent neural networks to probe neural dynamics. *Journal of Neurophysiology* 2019;122(6):2504–2521.
- [21] Yu BM, Cunningham JP, Santhanam G, Ryu S, Shenoy KV, Sahani M. Gaussian-process factor analysis for low-dimensional single-trial analysis of neural population activity. *Advances in neural information processing systems* 2008;21.
- [22] Chen RTQ, Rubanova Y, Bettencourt J, Duvenaud D. Neural Ordinary Differential Equations. *arXiv*; 2019.
- [23] Pei F, Ye J, Zoltowski D, Wu A, Chowdhury RH, Sohn H, et al. Neural Latents Benchmark '21: Evaluating latent variable models of neural population activity. *arXiv*; 2022.
- [24] Macke JH, Buesing L, Cunningham JP, Yu BM, Shenoy KV, Sahani M. Empirical models of spiking in neural populations. *Advances in neural information processing systems* 2011;24.
- [25] Gao Y, Archer E, Paninski L, Cunningham JP. Linear dynamical neural population models through nonlinear embeddings. *arXiv*; 2016.
- [26] Petreska B, Yu BM, Cunningham JP, Santhanam G, Ryu S, Shenoy KV, et al. Dynamical segmentation of single trials from population neural data. *Advances in neural information processing systems* 2011;24.
- [27] Brunton SL, Proctor JL, Kutz JN. Discovering governing equations from data by sparse identification of nonlinear dynamical systems. *Proceedings of the national academy of sciences* 2016;113(15):3932–3937.
- [28] Champion K, Lusch B, Kutz JN, Brunton SL. Data-driven discovery of coordinates and governing equations. *Proceedings of the National Academy of Sciences* 2019;116(45):22445–22451.
- [29] Bakarji J, Champion K, Kutz JN, Brunton SL. Discovering governing equations from partial measurements with deep delay autoencoders. *arXiv preprint arXiv:220105136* 2022;
- [30] Andalman AS, Burns VM, Lovett-Barron M, Broxton M, Poole B, Yang SJ, et al. Neuronal dynamics regulating brain and behavioral state transitions. *Cell* 2019;177(4):970–985.
- [31] Smith JTH, Linderman SW, Sussillo D. Reverse engineering recurrent neural networks with Jacobian switching linear dynamical systems. *arXiv*; 2021.
- [32] Maheswaranathan N, Williams A, Golub MD, Ganguli S, Sussillo D. Reverse engineering recurrent networks for sentiment classification reveals line attractor dynamics. *arXiv*; 2019.
- [33] Maheswaranathan N, Williams AH, Golub MD, Ganguli S, Sussillo D. Universality and individuality in neural dynamics across large populations of recurrent networks. *arXiv*; 2019.
- [34] Arneodo A, Coullet P, Tresser C. Occurrence of strange attractors in three-dimensional Volterra equations. *Physics Letters A* 1980 Oct;79(4):259–263. <https://www.sciencedirect.com/science/article/pii/0375960180903424>.
- [35] Golub MD, Sussillo D. FixedPointFinder: A Tensorflow toolbox for identifying and characterizing fixed points in recurrent neural networks. *Journal of Open Source Software* 2018;3(31):1003. <https://doi.org/10.21105/joss.01003>.
- [36] Rössler OE. An equation for continuous chaos. *Physics Letters A* 1976 Jul;57(5):397–398. <https://www.sciencedirect.com/science/article/pii/0375960176901018>.

- [37] Lorenz EN. Deterministic Nonperiodic Flow. *Journal of the Atmospheric Sciences* 1963 Mar;20(2):130–141. https://journals.ametsoc.org/view/journals/atsc/20/2/1520-0469_1963_020_0130_dnf_2_0_co_2.xml, publisher: American Meteorological Society Section: Journal of the Atmospheric Sciences.
- [38] Gilpin W. Chaos as an interpretable benchmark for forecasting and data-driven modelling. *Advances in Neural Information Processing Systems* 2021; <http://arxiv.org/abs/2110.05266>.
- [39] Paszke A, Gross S, Massa F, Lerer A, Bradbury J, Chanan G, et al. PyTorch: An Imperative Style, High-Performance Deep Learning Library. *arXiv*; 2019.
- [40] Liaw R, Liang E, Nishihara R, Moritz P, Gonzalez JE, Stoica I. Tune: A research platform for distributed model selection and training. *arXiv preprint arXiv:180705118* 2018;.
- [41] Poli M, Massaroli S, Yamashita A, Asama H, Park J. TorchDyn: A neural differential equations library. *arXiv preprint arXiv:200909346* 2020;.

Supplementary Material

6 | DATASETS

6.1 | Dynamical systems

6.1.1 | Arneodo

$$\dot{x} = y$$

$$\dot{y} = z$$

$$\dot{z} = -ax - by - cz + dx^3$$

where $a = -5.5$, $b = 4.5$, $c = 1.0$, and $d = -1.0$ [34].

6.1.2 | Rössler

$$\dot{x} = -y - z$$

$$\dot{y} = x + ay$$

$$\dot{z} = b + z(x - c)$$

where $a = 0.2$, $b = 0.2$, and $c = 5.7$ [36].

6.1.3 | Lorenz

$$\dot{x} = \sigma(y - x)$$

$$\dot{y} = x(\rho - z) - y$$

$$\dot{z} = xy - \beta z$$

where $\beta = 2.667$, $\rho = 28$, and $\sigma = 10$ [37].

6.2 | Solving and resampling latent trajectories

Systems were simulated using the `dysts` Python package, which offered well-reasoned standards for initial conditions, integration steps, and resampling frequency [38]. Initial conditions had been determined by running each model until the moments of the autocorrelation function were stationary. Integration steps had been chosen based on the highest significant frequency observed in the power spectrum (see Table 1). After integration, trajectories were resampled to contain a specified number of points per period (see Table 1), where period was defined based on the dominant frequency in each system's power spectrum.

TABLE 1 Dataset parameters and characteristics

System	Arneodo	Rössler	Lorenz
Solver step size (t)	1.215e-3	7.563e-4	1.801e-4
Points per period	35	35	70
Mean firing rate (spikes/bin)	1.624	1.872	1.695

7 | TRAINING DETAILS

All weights were initialized from $\mathcal{U}(-\sqrt{k}, \sqrt{k})$, where $k = 1/\text{in_features}$ for linear layers and $k = 1/\text{hidden_size}$ for GRU weights. Dropout layers ($p = 0.05$) were inserted before and after the IC linear projection during training. Loss was computed as the average Poisson NLL across neurons and time points and models were trained by gradient descent using Adam for 3000 epochs. Further training details for all models are given in Table 2.

TABLE 2 Training hyperparameters

	GRU	NODE
Batch Size	1280	1280
Learning Rate	1e-3	5e-3
Weight Decay	1e-4	1e-5

8 | FINDING FIXED POINTS

For each network, fixed points were located by randomly sampling 1024 initial states from inferred latent trajectories and iteratively minimizing the squared norm of the vector field [9]. We used Adam with a learning rate of 1e-2 for minimization over 5000 iterations. Uniqueness was determined using a distance threshold of 1e-3 and points that did not achieve a squared norm less than 1e-10 were excluded. In practice, there were many orders of magnitude between kept and excluded points.

9 | COMPUTE RESOURCES

We used an internal computing cluster with a total of 30 NVIDIA GeForce RTX 2080 Ti GPUs for model training. Each model took approximately 3 hours to train. With 2 models training on each GPU, the 210 models took approximately 10.5 hours.

10 | METRICS

10.1 | Rate reconstruction

We computed the coefficient of determination between true (r) and predicted (\hat{r}) rates for each neuron, and reported the average value across neurons. We refer to this metric as rate R^2 .

$$R^2 = \frac{1}{N} \sum_{i=0}^N 1 - \frac{\sum (r_i - \hat{r}_i)^2}{\sum (r_i - \bar{r}_i)^2}$$

10.2 | Hidden reconstruction

To compute hidden R^2 , we concatenated a vector of ones to the true latent states (L_1), then used the pseudoinverse to find a set of weights that produced an affine transform from the true latents to the hidden states (H) with minimal squared error. We computed R^2 for this projection as described in the previous section.

$$\hat{H} = L_1 L_1^\dagger H$$

11 | OPEN-SOURCE PACKAGES USED

- `torch` [39] (BSD license): Deep learning framework providing layer definitions, GPU acceleration, automatic differentiation, optimization, and more.
- `pytorch_lightning` (Apache 2.0 license): Lightweight wrappers for model training.
- `ray.tune` [40] (Apache 2.0 license): Distributed hyperparameter tuning.
- `dysts` [38] (Apache 2.0 license): Implementations for modeled dynamical systems.
- `torchdyn` [41] (Apache 2.0 license): Implementation of NODEs.
- `fixed_point_finder` [35] (Apache 2.0 license): Inspiration for `torch`-based fixed point finder.